

Isotope Shift of Nuclear Charge Distributions*

K. A. BRUECKNER, WING-FAI LIN, AND R. J. LOMBARD†

*Department of Physics and Institute for Pure and Applied Physical Sciences, University of California, San Diego,
La Jolla, California 92037*

(Received 23 January 1969)

The energy-density formalism is applied to the study of the isotope shift of nuclear charge distributions. It allows us to determine the part of the shift due to a statistical change in the proton densities. The study is improved by a shell-model calculation based on the Thomas-Fermi potential. The charge distributions are in relatively good agreement with experiment. However, the present model cannot reproduce the part of the shift due to nonmonotonic changes in charge distributions. These nonmonotonic effects are of a more complicated origin; they are of the same order of magnitude as the statistical shifts. In the case of the pair of Ca⁴⁰-Ca⁴⁸ our results are consistent with shifts calculated in self-consistent (Hartree-Fock) methods.

I. INTRODUCTION

THE accuracy of experiments on charge distributions in nuclei by means of muonic x rays and electron scattering has been improved greatly in recent years.¹ Density expressions with parameters adjusted for the best fit to experimental results indicate that changes in charge distributions of isotopes deviate from the $A^{1/3}$ law and show nonmonotonic variations with the mass number.

Several recent calculations have attempted to explain isotope shifts on the basis of the nuclear shell model.² Phenomenological potentials have been used with parameters chosen so as to yield the known shell structure, the binding energies of the last few nucleons, and the best fit to the electron-scattering data, taking density distributions based on single-particle wave functions. Various refinements of the calculations have been reported, but they are all empirical to some extent.

The energy-density formalism developed by Brueckner *et al.*³ provides a practical method for studying variations in shape and size of proton and neutron distributions as a function of N and Z . Obviously a statistical approach is not supposed to reproduce nonmonotonic effects which originate from the shell structure and correlations between the nucleons. However, the method allows the precise estimation of the isotope shift due to statistical changes in the mean potential and separates it from contributions having a more complex origin.

On the other hand, the statistical theory can be

improved by a shell-model calculation in which the shell-model potential is approximated by the Thomas-Fermi potential. Strictly speaking, this is the potential experienced by the last bound nucleon. However, as we shall see in Sec. III, this approximation turns out to be sufficient for the states lying within one to two major shells from the Fermi surface. In other words, it is certainly as good as any phenomenological Woods-Saxon potential and the statistical theory yields, at least, reliable predictions of the variations of the potential from one nucleus to the other.

Isotope shifts have been calculated for three pairs of isotopes, namely, Ca⁴⁰-Ca⁴⁸, Sn¹¹⁶-Sn¹²⁴, and Pb²⁰²-Pb²⁰⁸. This choice is dictated partly by existing experimental data. The above shifts are small; it is easier to study cases with a large difference in the neutron number. The results will be compared with experimental data and discussed in Sec. IV.

II. DENSITY DISTRIBUTIONS FROM STATISTICAL THEORY

The main purpose of the energy-density formalism is to replace the set of self-consistent equations describing the ground state of a many-nucleon system by a functional $E[\rho(r)]$ of the local density $\rho(r)$. A detailed derivation of the functional is given in previous papers,³ so we merely want to outline its form:

$$E[\rho] = \int \mathcal{E}[\rho(r)] d^3r,$$

$$\mathcal{E}[\rho] = \frac{3}{8}(\hbar^2/2M) \left(\frac{3}{2}\pi^2\right)^{2/3} \left\{ \frac{1}{2}[(1-\alpha)^{5/3} + (1+\alpha)^{5/3}] \right\} \rho^{5/3} + \rho V(\rho, \alpha) + \frac{1}{2}e\rho_p\phi_c - 0.7386e^2\rho_p^{4/3} + (\hbar^2/8M)\eta(\nabla\rho)^2,$$
(1)

with $\rho(r) = \rho_p(r) + \rho_n(r)$.

The densities are subject to the conditions

$$\int \rho_p(r) d^3r = Z, \quad \int \rho_n(r) d^3r = N. \quad (2)$$

* Research supported by the U.S. Atomic Energy Commission under Contract No. AT(11-1)-GEN-10, P.A. 11.

† Permanent address: Institut de Physique Nucléaire, Division de Physique Théorique, laboratoire associé au CNRS, 91-Orsay, France.

¹ An outstanding review of experimental data can be found in *Nuclear Radii* (Landolt-Börnstein, Springer Verlag, New York, 1967).

² F. G. Perey and J. P. Schiffer, *Phys. Rev. Letters* **17**, 324 (1966); L. R. B. Elton, *Phys. Rev.* **158**, 970 (1967); B. F. Gibson and K. J. van Oostrum, *Nucl. Phys.* **A90**, 159 (1967); H. A. Bethe and L. R. B. Elton, *Phys. Rev. Letters* **20**, 745 (1968).

³ K. A. Brueckner *et al.*, *Phys. Rev.* **171**, 1188 (1968); **173**, 944 (1968).

The neutron excess is defined as

$$\alpha(r) = [\rho_n(r) - \rho_p(r)] / \rho(r). \quad (3)$$

The first term in the functional represents the KE. The potential energy is expressed by the second term, which is directly derived from a nuclear-matter calculation with variable neutron excess by Brueckner *et al.*⁴ It should be noticed that the results may depend on the nuclear-matter calculation. However, it lies outside the scope of the present work to study this dependence, and we therefore restrict ourselves to the case of the Brueckner-Gammel-Thaler potential used in Ref. 4, which has been proved to be very successful in deriving gross properties of nuclei. The third and the fourth terms are the Coulomb and the exchange Coulomb energy, respectively, ϕ_c being the Coulomb potential. The last term takes care of the finite range of the nuclear force. There is some arbitrariness in the choice of the parameter η , which is fixed to give an experimental binding energy. In the present case the criterion is the binding energy of Ca⁴⁰. However, isotopic changes of charge distributions are not sensitive to variation of η over a reasonable range.

The ground-state density is obtained in seeking the two functions $\rho_p(r)$ and $\rho_n(r)$ minimizing expression (1). The problem can be solved either in considering the Lagrange-type differential equations associated with (1) or variationally using convenient trial functions for $\rho_p(r)$ and $\rho_n(r)$. It was shown in Ref. 3 that the closest agreement with the solutions of the differential equations is obtained with the so-called modified Gaussian distributions multiplied by third- (or fourth-) order polynomials:

$$\rho_{p,n}(r) = \rho_0(1 + pr^2 + tr^3) \{1 + \exp[(r^2 - R^2)/B^2]\}^{-1}. \quad (4)$$

Other functions such as the so-called three-parameter Fermi distributions, for instance, are insufficiently general. The variational method consists of seeking the two sets of parameters (R , B , p , t) giving the largest binding energy. It is interesting to note that a small negative value of the parameter t is needed, because in the Thomas-Fermi approximation the density which minimizes the energy functional has to have its point of steepest slope at a larger radius than the half-density point. The constants ρ_{0p} and ρ_{0n} are determined by the conditions on the numbers of protons and neutrons, respectively.

The proton and neutron distributions have been calculated for Ca⁴⁰, Ca⁴⁸, Sn¹¹⁶, Sn¹²⁴, Pb²⁰², and Pb²⁰⁸. For Ca and Sn isotopes, η has been set equal to 8, whereas for Pb a slightly lower value, namely, 7.5, has been used. An r^3 term in the polynomial is used for the Ca isotopes, which is replaced by r^4 for the Sn and Pb.

TABLE I. Results of the energy-density formalism obtained with modified Gaussian distributions. A third-order polynomial is used for the Ca isotopes, whereas in the case of Sn and Pb the r^3 term is replaced by r^4 . The parameter η is chosen to be 8 for Ca and Sn and 7.5 for Pb. Comparison is made with experimental charge distributions of the Fermi type.

(a)	Theory		Experiment	
	$r_{0.5}$	t	$r_{0.5}$	t
Ca ⁴⁰	3.640	2.42	3.58	2.65
Ca ⁴⁸	3.805	2.38	3.74	2.30
Sn ¹¹⁶	5.270	2.22	5.28	2.37
Sn ¹²⁰			5.32	2.53
Sn ¹²⁴	5.385	2.22	5.44	2.37
Pb ²⁰²	6.540	1.95		
Pb ²⁰⁸	6.605	1.95	6.7	2.0
(b)		$\Delta r = \Delta r_{0.5} / r_{0.5}$		
	Experiment	Statistical theory	$A^{1/3}$ law	
Ca ⁴⁰ -Ca ⁴⁸	4.4%	4.5%	6.3%	
Sn ¹¹⁶ -Sn ¹²⁴	3%	2.2%	2.2%	
Pb ²⁰² -Pb ²⁰⁸		1.0%	1.0%	

The corresponding proton distributions are plotted in Fig. 1. The results are also expressed in terms of proton half-density radius $r_{0.5}$ and proton surface thickness t (defined as the distance over which the density drops from 90% to 10% of its central value). They are summarized in Table I(a) and compared to the experimental data. As we can see the agreement is satisfactory although the surface thicknesses are 5–10% too small, except in the case of Ca⁴⁸. In the case of Ca isotopes, the change in the surface thickness t is about half of its experimental value.

It is interesting to compare the relative changes in the half-density radii with the predictions of the $A^{1/3}$ law. In this later case, the half-density radius is given by

$$r_{0.5} = r_0 A^{1/3}, \quad (5)$$

where r_0 is a constant. According to this, the relative change in $r_{0.5}$, defined as

$$\Delta r = \Delta r_{0.5} / r_{0.5}^{(1)} = (A_2^{1/3} - A_1^{1/3}) / A_1^{1/3} \quad (6)$$

is independent of r_0 . The different values are given in Table I(b). Apart from the Ca case, the statistical theory yields results for Δr in close agreement with the $A^{1/3}$ law. This can be understood in light of earlier results on half-density radii. Except for a dip in the 40–60 mass region, as found in experiments, $r_{0.5}$ from statistical theory obeys an $A^{1/3}$ law rather well.³ This follows from the fact that an increase in the radius of

⁴ K. A. Brueckner *et al.*, Phys. Rev. **168**, 1184 (1968).

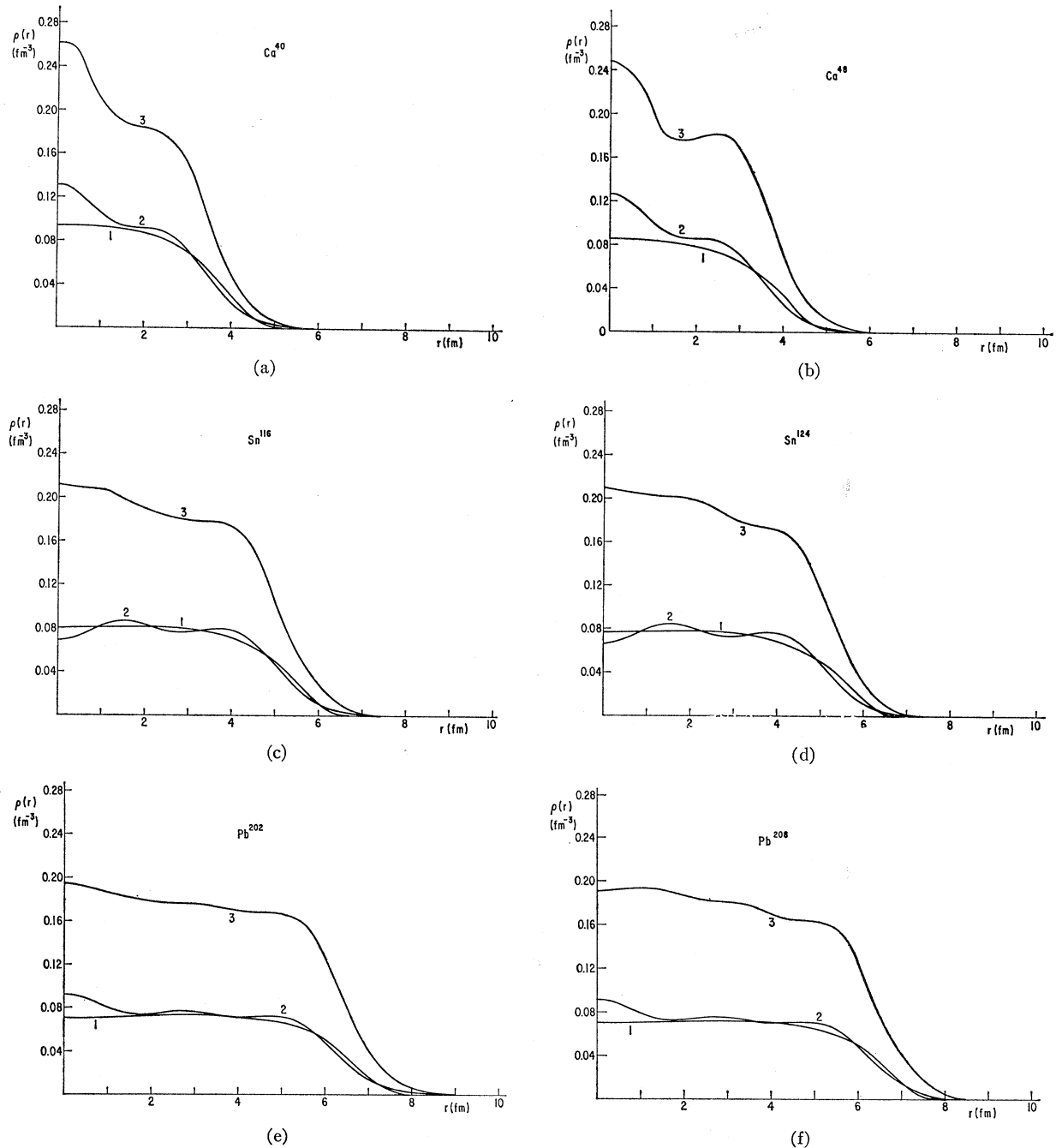


FIG. 1. Nucleon densities for isotopes of Ca, Sn, and Pb. In each figure, curve 1 is the proton density from statistical theory (see also the caption of Table I), while curves 2 and 3 are the shell-model proton and mass densities, respectively.

the neutron distribution increases the radius of the nuclear potential seen by a proton, thus causing a very nearly comparable increase in the radius of the proton distribution.

The rms radii of proton distributions r_p are very sensitive to the tails of the distributions. Therefore, the statistical theory is not suitable to study small changes

in r_p . This quantity will be discussed in more detail in the shell-model estimate.

III. SHELL EFFECTS

The next step towards a better understanding of the isotope shift of nuclear charge distributions consists in taking into account the shell structure. This will be

TABLE II. Comparison of calculated eigenvalues (in MeV) of a few states close to Fermi surface of Ca⁴⁰ with results from ML^a and experiments.^b $\lambda = 30$.

State	This paper		ML		Experimental	
	Neutron	Proton	Neutron	Proton	Neutron	Proton
1d _{5/2}	-20.08	-12.74	-17.5	-10.3	-21.78	-14.69
2s _{1/2}	-15.91	-8.55	-14.8	-7.6	-18.10	-10.87
1d _{3/2}	-14.31	-6.45	-12.6	-5.5	-15.63	-8.34
1f _{7/2}	-8.94	-1.88			-8.36	-1.08

^a Reference 6.

^b Reference 7.

done here in a simple way; the shell-model average field is approximated by the Thomas-Fermi potential, and the densities are obtained by adding the corresponding single-particle densities.

A. Shell-Model Potential

The mean potential $U_n(r)$ [$U_p(r)$] experienced by the last bound neutron (proton) is given by the functional derivative of the total potential energy with respect to $\rho_n(r)$ [$\rho_p(r)$]. The corresponding shell-model potential $V_n(r)$ [$V_p(r)$] is obtained by adding a Thomas-type spin-orbit term with a strength parameter λ , e.g.,

$$V_n(r) = U_n(r) - \lambda \frac{1}{2} (\hbar/mc)^2 (1/r) (\partial/\partial r) U_n(r) \mathbf{l} \cdot \mathbf{s}, \quad (7)$$

where the factor \hbar/mc is the nucleon Compton wavelength. The same strength parameter λ has been used for both neutrons and protons. Its value is taken to be 30 in order to give a good fit to the available experimental data on separation energies, level sequences, spin-orbit splittings, and level spacings for the states

close to the Fermi surface, namely, the single-particle energies in Ca⁴⁰, Ca⁴⁸, and Pb²⁰⁸. This choice is consistent with values used in previous calculations based on Woods-Saxon potentials.⁵

The statistical theory breaks down at low density. In order to get rid of this difficulty a potential tail of Woods-Saxon form is fitted to $U_n(r)$, [$U_p(r) - e\phi_c + \frac{4}{3}(0.7386e^2)\rho_p^{1/3}$, i.e., the nuclear well for a proton], when $\rho_p(r)$ is less than $0.15 \times \rho_p(0)$, the first two derivatives of the potential being made continuous. Since isotopic shifts are small and since proton densities usually vanish more quickly than neutron densities, it is essential to have the proton wells of each isotopic pair fitted with tails at approximately equal proton densities. Typical results, the potentials for Ca⁴⁰ and Pb²⁰⁸, are shown in Fig. 2.

The calculated energy eigenvalues are given in Tables II–V. Comparisons with results from other calculations, e.g., Masterson and Lockett,⁶ and with experiment⁷ are made when possible. We stay in the local-field approximation and ignore the state dependence of the shell-model potential, a point which we shall

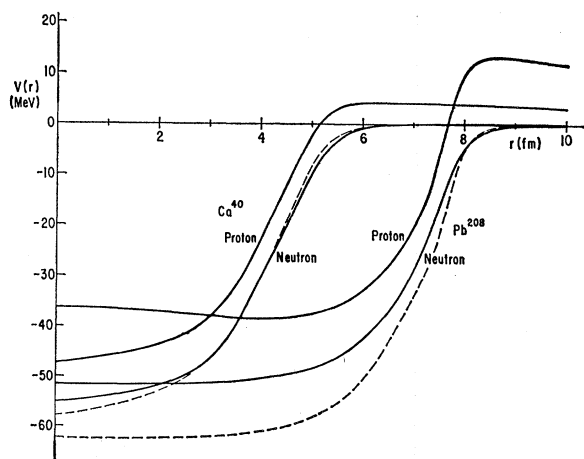


FIG. 2. S-state neutron and proton single-particle potentials for Ca⁴⁰ and Pb²⁰⁸. Dashed curves are proton nuclear wells. The increase in potential depth for protons is the result of the symmetry terms in the energy density, the protons interacting strongly with the excess neutrons.

TABLE III. Comparison of calculated eigenvalues (in MeV) of a few states close to Fermi surface of Ca⁴⁸ with results from experiments.^a $\lambda = 30$.

State	This paper		Experimental	
	Neutron	Proton	Neutron	Proton
1d _{3/2}	-14.54	-13.25	-12.40	-15.26
1f _{7/2}	-8.99	-8.36	-9.94	-9.62
2p _{3/2}	-4.16		-5.14	

^a Reference 7.

⁵ See, e.g., A. A. Ross, H. Mark, and R. D. Lawson, Phys. Rev. **102**, 1613 (1956); M. Blomquist and M. Wahlborn, Arkiv Fysik **16**, 545 (1965); M. Bleuler, M. Beiner, and M. de Tourreil, Nuovo Cimento **52**, 45 (1967).

⁶ K. S. Masterson, Jr., and A. M. Lockett, Phys. Rev. **129**, 776 (1963).

⁷ See *Nuclear Data Sheets* [compiled by K. Way *et al.* (Academic Press Inc., New York, 1965)] as well as G. Sartoris and L. Zamick [Phys. Rev. **167**, 1035 (1968)] for levels in Ca⁴⁸.

TABLE IV. Comparison of calculated eigenvalues (in MeV) of a few states close to Fermi surface of Pb²⁰⁸ with results from ML^a and experiments.^b $\lambda = 30$.

State	This paper		ML		Experimental	
	Neutron	Proton	Neutron	Proton	Neutron	Proton
$1h_{11/2}$	-17.05	-7.41	-21.2	-8.9		-9.37
$2d_{3/2}$	-17.88	-6.40	-22.6	-10.4		-8.53
$3s_{1/2}$	-17.72	-6.02	-22.5	-9.7		-8.03
$1h_{9/2}$	-12.08	-1.38	-15.6			-3.77
$2f_{7/2}$	-12.14		-13.5			
$1i_{13/2}$	-9.79		-9.2		-9.16	
$3p_{3/2}$	-9.54		-10.9		-8.39	
$2f_{5/2}$	-9.15		-10.3		-8.05	
$3p_{1/2}$	-8.34		-8.8		-7.38	
$2g_{9/2}$	-4.41				-3.94	

^a Reference 6.^b Reference 7.

return to in Sec. IV. Nevertheless the results show that the above approximation is sufficient for states close to the Fermi surface, while the potential energy is too low for the deeper states.

The choice of λ and the potential matching point are subject to some arbitrariness. However, we have verified that the energy eigenvalues, rms radii of densities, and isotope shifts are not sensitive to these uncertainties. This implies that the low-density part has now been established with enough accuracy which is particularly important when comparing the rms radii of charge distribution r_c . The level sequencies are affected when level separations are small.

B. Shell-Model Densities

Shell-model neutron and proton densities are obtained by adding single-particle contributions. In cases where the neutron subshells are not completely filled, as in Sn¹²⁴ and Pb²⁰², we make an angular average to obtain the radial neutron densities. Proton and mass distributions calculated in the present work are plotted in Fig. 1. In the proton case, the results of the energy-density formalism are also plotted for comparison. It can be seen that the results from the two approaches are consistent with each other: The statistical density is averaging the single-particle estimate. The corresponding charge distributions result from folding the finite distribution of the proton:

$$\rho_F(r) = \pi^{-3/2} a_F^{-3} \exp(-r^2/a_F^2), \quad (8)$$

(with $a_F = 0.65$ fm) into the distribution of proton centers in the nuclei.⁸

⁸ L. R. B. Elton and A. Swift, Nucl. Phys. A94, 52 (1967).

The calculated and experimental values are given in Table VI.

IV. DISCUSSION

The energy-density formalism enables us to calculate that part of the isotope shift arising from a statistical change in proton distributions. Nonmonotonic effects appear to be of the same order of magnitude. They have a different origin and require a more sophisticated theory.

The shell-model calculations based on the Thomas-Fermi potential confirm the results obtained directly from the energy-density formalism. As far as the rms radii of the proton distributions are concerned, this is necessary to remove the uncertainties related to the tails of the distributions.

Because of the omission of the state dependence of the shell-model potential, we expect the total shell-model density distributions to be less accurate than the changes in density. Thus the calculated isotope shifts should be dependable, since the effect relies to a large extent on the change in density distributions due

TABLE V. Calculated eigenvalues (in MeV) of a few states close to Fermi surface of Pb²⁰², $\lambda = 30$.

Neutron state	Eigenvalue	Proton state	Eigenvalue
$1h_{9/2}$	-11.89	$2d_{5/2}$	-7.35
$1i_{13/2}$	-9.66	$1h_{11/2}$	-6.21
$3p_{3/2}$	-9.59	$2d_{3/2}$	-5.13
$3f_{5/2}$	-9.12	$3s_{1/2}$	-4.78

TABLE VI. Shell-model rms proton r_p , mass r_m , and charge r_c radii (in fm) are compared with results from statistical theory and experiments^a (see also Ref. 9).

Nucleus	Statistical theory		Shell model			Experimental			$A^{1/3}$ scaling	
	r_p	r_m	r_p	r_m	r_c	$\delta r_c/r_c$	r_c	$\delta r_c/r_c$		
Ca ⁴⁰	3.12	3.11	3.200	3.185	3.298	0.73%	3.50 ^b	3.41 ^e	-0.3% ^b	6.3%
Ca ⁴⁸	3.20	3.25	3.225	3.353	3.322		3.49 ^b	3.39 ^e		
Sn ¹¹⁶	4.28	4.31	4.354	4.385	4.427	0.63%	4.55 ^b	4.50 ^d	2.6% ^b	
Sn ¹²⁴	4.34	4.40	4.384	4.448	4.455		4.67 ^b	4.60 ^d		
Pb ²⁰²	5.16	5.20	5.199	5.278	5.260	0.46%	5.49 ^b		1.0%	
Pb ²⁰⁸	5.20	5.25	5.224	5.311	5.284					

^a Reference 1.^b Corresponds to Fermi distributions.^e Corresponds to Woods-Saxon distributions.^d Corresponds to Gaussian distributions.

to few upper states for which our potentials should be sufficiently accurate.

The calculated values of the rms radii are summarized in Table VI together with the experimental results and the predictions of $A^{1/3}$ scaling. The shell-model predictions give considerably smaller radius increases than the $A^{1/3}$ scaling, particularly for Ca⁴⁰-Ca⁴⁸, where the calculation gives a small increase (0.73%), while $A^{1/3}$ scaling gives 6.3%. This result agrees qualitatively with the experimental result which actually gives a slight decrease in rms radius of the charge distribution.⁹ The shell-model prediction of +0.63% for the tin isotope pair, which again is considerably less than the $A^{1/3}$ scaling (2.2%), now disagrees with the experimental result which in this case follows the $A^{1/3}$ scaling closely.¹⁰ The prediction for the lead isotopes is also for considerably less increase in rms radius than from $A^{1/3}$ scaling. No results are available, however, for the isotope pair considered, although Anderson *et al.*¹¹ found a negative Δr_c (rms) [defined similar to Eq. (6)] in going from Pb²⁰⁶ to Pb²⁰⁸, a result which has been confirmed by Ehrlich *et al.*¹²

Adjusting the nuclear-matter saturation curve to obtain more consistent binding energies gives statistical theory results slightly different from those used above, as reported by Brueckner *et al.*³ With these new results, the shell-model calculations have been repeated for the Ca isotopes, giving an isotopic shift close to that reported above.

⁹ R. F. Frosch, R. Hofstadter, J. S. McCarthy, G. K. Nöldeke, K. J. van Oostrum, M. R. Yearian, B. C. Clark, R. Herman, and D. G. Ravenhall (unpublished); earlier results are found in Ref. 1.

¹⁰ P. Barreau and J. B. Bellicard, Phys. Letters 25B, 470 (1967).

¹¹ H. L. Anderson, R. J. McKee, C. K. Hargrove, and E. P. Hincks, Phys. Rev. Letters 16, 434 (1966).

¹² R. D. Ehrlich, D. Fryberger, D. A. Jensen, C. Nissim-Sabat, R. J. Powers, B. A. Sherwood, and V. L. Telegdi, Phys. Rev. Letters 18, 959 (1967); Phys. Letters 23, 468 (1966).

As we have already said in Sec. I, the statistical theory can only determine the isotope shift due to statistical changes in the mean potential. Nonmonotonic variations have a more complex origin, and apparently are not given with sufficient accuracy by the improvement over the statistical method resulting from the calculation of the single-particle states in the Fermi-Thomas field. Our results, in fact, mainly confirm and improve the statistical results. Actually both calculations of the rms radii are close to each other. Thus the origin of isotope shifts appears to lie in details of the nuclear potential and of nucleon correlations outside of the scope of the present simplified theory.

The weak point in the formalism is that the shell structure is not taken into account in determining the shell-model potential. This, of course, is the basic failure of the energy-density formalism. From this point of view, it is interesting to compare with other self-consistent calculations. In fact, the Ca⁴⁰-Ca⁴⁸ isotope shift has become a challenge, and various authors have tried to reproduce the negative Δr_c (rms). Using a Hartree-Fock calculation developed on a harmonic-oscillator basis, Tarbuton and Davis¹³ get +1.0%. Other self-consistent calculations based on simple effective interactions yield equivalent results, namely, +1.7% for Köhler¹⁴ and +1.2% for Pirès *et al.*¹⁵ In contrast, a Hartree-Fock calculation using the Tabakin potential, without a Coulomb force, gives -6.5%¹⁶; including the Coulomb potential should not affect the main feature of this result.

¹³ R. M. Tarbuton and K. T. R. Davis, Nucl. Phys. A120, 1 (1968).

¹⁴ H. S. Köhler (private communication).

¹⁵ P. Pirès, R. de Turrell, D. Vautherin, and M. Vénéroni, Contribution to the Dubna Symposium on Nuclear Structure, 1968 (unpublished).

¹⁶ J. P. Svenne (private communication).